Journal of Mineralogical and Petrological Sciences, Volume 95, page 182-192, 2000

Thermal expansion of alumnus perovskite $ScAlO_3$

Takamitsu YAMANAKA*, Robert C. LIEBERMANN** and Charles T. PREWITT***

*Department of Earth and Space Science, Graduate School of Science Osaka University
1-1 Machikaneyama Toyonaka, Osaka 560-0043 JAPAN
** Space and Planetary Sciences State University of New York at Stony Brook Stony Brook,
New York 11794-2100
***Geophysical Laboratory, Carnegie Institution 5251 Broad Branch Road, N.W. Washington. D.C. 20015

Thermal structure deformation of $ScAlO_3$ perovskite was studied by in situ X-ray single crystal structure analysis at high temperatures. As temperature increases, all structure parameters of the orthorhombic perovskite shift very slightly toward the ideal polyhedral symmetries. The cell volume shows a quadratic thermal expansion expressed by $V(T)/V_{293}=1+1.151\times10^{-5}T+9.218\times10^{-9}T^2$. The expansions of ScO_8 and void space are significant for the cell volume expansion because they occupy large volume in the unit cell. The tilting and rotation of AlO_6 octahedral linkage are a little changed by the anisotropic thermal motion of O1 and O2. Higher order anisotropic anharmonic thermal parameters of γ_{pqr} and δ_{pqrs} of O1 and O2 atoms are increased noticeably with temperature. Anharmonic motions of oxygen atoms, inducing the tilting and rotation of AlO_6 octahedra mainly control the thermal changes of perovskite structure.

Introduction

Since the first remark by Ringwood (1962) of the possible importance of $MgSiO_3$ and $CaSiO_3$ perovskites in the lower mantle science, many studies on high-pressure transformations of metasilicates have been conducted for geophysical interpretation (Liu, 1978; Ito and Matsui, 1978; Yagi et al. 1978). Crystal chemical significance of silicate perovskite has been discussed by Sinclair (1979); Knittle et al. (1986), Yagi et al. (1978), Kudoh et al. (1987) and Ross and Hazen, (1990). Aluminate perovskite also attracts a large attention in relation with the possible aluminum reservoir in the lower mantle.

Another major geophysical interest in mantle science is the phase stability of various perovskite polymorphs, such as germanates, titanates and aluminates (Sasaki et al. 1983; Susaki et al. 1985; Reid and Ringwood, 1975). Rare earth aluminate perovskites ($ReAlO_3$) have been extensively studied from the ferroelectric or piezoelectric interests. The perovskite-type polymorphs of $LaAlO_3$, $CeAlO_3$, $PrAlO_3$ and $NbAlO_3$ have trigonal symmetry. The crystal structures of orthorhombic $SmAlO_3$ and of trigonal $NbAlO_3$ have been studied at room temperature (Merezio et al. 1972).

It has been known from the previous studies that the general trend of perovskites transformation with elevating temperature is toward rhombohedral ($R\bar{3}c$)→ orthorhombic (Pbnm)→ tetragonal (I4/mcm)→ cubic (Pm3m) or hexagonal (P6/mmc) structure. Many perovskite polymorphs in the earth materials may exhibit the same trend. The structural deformation is classified by cation displacement and tilting of octahedra (Galasso, 1970; Glazer, 1972, 1975). The deformations, on heating and compression, induce the transformation of the crystal. Previously the metrical discussions with respect to perovskite structures were repeated. Based on the assumption that BX_6 octahedra take a regular form in ABX_3 perovskite structures, the lattice constant and unit cell volume of distorted perovskite could be readily calculated from the idealized cubic perovskite (Zhao et al. 1993a, 1993b).

Among many aluminate perovskites, $ScAlO_3$ bears an important meaning for geophysical implication as a model composition of $(Mg_{1-x}Fe_x)SiO_3$ perovskite in mantle, because the Sc^{3+} (r=0.73Å) is intermediate size between Mg^{2+} (r=0.72Å) and Fe^{2+} (r=0.77Å), and octahedral Al^{3+} (r=0.53Å) does not greatly exceed that

T. Yamanaka, 山中高光, b61400@center.osaka-u.ac.jp Corresponding Author
R.C. Liebermann, robert.libermann@sunnysb.edu
C.T. Prewitt, prewitt@gl.ciw.edu

of Si^{4+} (r=0.53Å) (Reid and Ringwood, 1975). Bulk and shear moduli of aluminates correlate with distortion from cubic symmetry and tilting angles of the AlO_6 octahedra (Bass, 1984). Applying Rietveld profile fitting method on their powder diffraction data, Hill and Jackson (1990) investigated the thermal expansion of $ScAlO_3$ up to 1100°C. They discussed the geophysical implications from their results. In a high-pressure structure refinement of $ScAlO_3$ (Ross, 1998), the distortion of the structure shows neither significant change nor tilting of octahedral chains with increasing pressure.

Previous studies of ABO_3 perovskite structures and their physical properties generally paid attention only to the BO_6 octahedral linkage. The present experiment has elucidated the thermal structure deformation of the individual cation sites, AO_8, BO_6 and void space in the unit cell. The present X-ray single crystal structure analysis investigated the $ScAlO_3$ perovskite structure as a function of temperature. It was concluded that anharmonic thermal vibrations of atoms caused the structural change. The thermal vibration induces the volume expansion of the cation site.

Experimental

High temperature heating system

The development of high-temperature crystallography owes to the progress in heating devices. Many types of heating equipment such as electric resistance heater (Brown et al, 1973), gas flame heater (Yamanaka et al. 1981) and laser heating system have been reported for X-ray diffraction studies in the temperature range up to 2000°C(Yamanaka and Takeuchi, 1983). The common heater is the electric-resistance heater. However, several difficulties such as the oxidation of sample, regulation of sample temperature and the blind region in the reciprocal space were encountered. In order to overcome these problems, a heated gas apparatus has been devised for X-ray structure analysis (Figure 1). This system was installed on a four-circle diffractometer. Heated nitrogen gas was introduced into a small spherical glass bulb, in which the crystal sample was placed at the center. The apparatus realized a stable temperature and wide isothermal region around the sample. Temperature was controlled by PID electric controlling system and by gas-flow regulation. The use of nitrogen gas protects the sample from oxidation even at high temperature. It offers another advantage to cover the full 2θ diffraction range because there is no blind region for the diffraction intensity measurement.

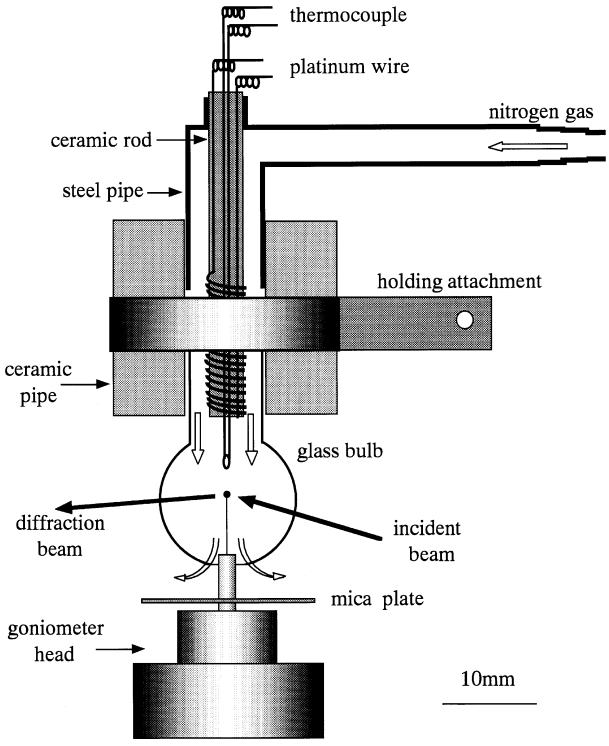

Figure 1 Heated gas apparatus.
Heated nitrogen gas is introduced into the small spherical glass bulb, which is installed on the four-circle goniometer. The temperature regulation is conducted by PID electric controlling system and by gas-flow rate.

X-ray crystal structure refinement

The $ScAlO_3$ single crystals used in the present structure refinement were the same samples as used for the measurement of elastic moduli by Bass (1984). X-ray diffraction intensities were collected by a four-circle diffractometer with MoKα radiation (λ=0.71069Å) and ω-2θ scanning bisecting mode. A 2θ scanning speed of 2° min^{-1} and scanning width of 1.5°+0.5°tanθ were applied for the data collection. Data were collected at four different temperatures, 20, 192, 440 and 703°C. A temperature fluctuation at the highest temperature was less than ±10°C.

Reflections having of $F_o > 3\sigma$ F_o within 0.1 $Å^{-1} < \sin\theta/\lambda < 1.32$ $Å^{-1}$ were used for the refinement. The intensities were corrected for Lorentz and polarization effects and prismatic absorption. Cell dimensions of $ScAlO_3$ were determined by the least-squares procedure applying, 2θ values of 25 independent reflections falling within the $40° < 2\theta < 50°$. The lattice constants thus obtained are presented in Table 1.

The structure refinement using each data set has been conducted by the full matrix least-squares program RADY written by Sasaki (1987). Atomic scattering

Table 1. Lattice constants and cell volume

temperature	20° C	192° C	440° C	703° C
a (Å)	4.9355(15)	4.9425(20)	4.9535(6)	4.9691(27)
b (Å)	5.2313(13)	5.2343(29)	5.2436(9)	5.2525(33)
c (Å)	7.2003(6)	7.2043(36)	7.2157(11)	7.2273(31)
V (Å^3)	185.905(6)	186.379(1)	187.432(1)	188.634(2)
$\sqrt{2}$ a/c	0.9694	0.9694	0.9704	0.9723
$\sqrt{2}$ b/c	1.0275	1.0275	1.0273	1.0278
a/b	0.9435	0.9437	0.9447	0.9460

factors for neutral atoms were taken from International Tables for X-ray Crystallography, Vol. IV (1974).

At the first stage of data processing, atomic coordinates, anisotropic temperature factors and isotropic extinction parameter were chosen as the variable parameters. Initial structure parameters were referred from Sinclair, Eggleton and Ringwood (1979). Experimental conditions for diffraction intensity measurements are listed in Table 1. The reliability factor of the least-squares refinement is defined as $R=\sum | F_c^{2-} F_o^2 | / \sum | F_o^2 |$. The refined structure parameters, including an isotropic temperature factor B_{iso}, at each temperature are presented in Table 2. Atomic displacements from the ideal positions, i.e. crystallographic special positions ($x_0y_0z_0$), are presented by Δ(Å) in the table.

$$\Delta(\text{Å})=\sqrt{a^2(x_i-x_0)^2+b^2(y_i-y_0)^2+c^2(z_i-z_0)^2} \quad (1)$$

After the above structure refinement, anharmonic thermal parameters were also refined on the basis of the following Gram-Charier expansion (Johnson and Levy, 1974) in consideration of site symmetry restrictions on thermal-motion tensor coefficients, given in International Tables for X-ray Crystallography, Vol. IV (1974) as

$$T(h)=\exp(-\beta_{pq}h_ph_q)[1+\{2\pi i)^3/3\,!\,\}\gamma_{pqr}h_ph_qh_r+\{2\pi i)^4/4\,!\,\}\delta_{pqrs}h_ph_qh_rh_s+\ldots.], \quad (2)$$

where β_{pq}, γ_{pqr} and δ_{pqrs} coefficients denote second, third and fourth polar tensors, respectively and h indicates the reflection index.

The structure factor F(h) of reflection h is expressed by

$$F(h)=\Sigma f_i\exp(2\pi i\Sigma h_p x_{pi})T(h) \quad (3)$$

where f_i represents the atomic scattering factor of atom i, x_{pi} with p=1 to 3 is an atomic coordinate (xyz) of atom i and h_p (p=1 to 3) denotes a reflection (hkl).

Temperature factors up to fourth-rank coefficients are meaningful in the present least-squares refinement. The coefficients over 5th rank correlated so strongly each other to permit us to truncate in this procedure. We refined for the fourth rank coefficients, only three coefficients, δ_{1111}, δ_{2222} and δ_{3333} were refined in all atoms and others were set to be zero because of negligible or meaningless magnitudes in comparison with the standard deviations. The converged temperature factors are presented in Table 3. The temperature factor T(h) can be explained by the Fourier transform of the probability density function P(u) of atomic thermal displacement (u).

$$T(h)=\int P(u)\exp(2\pi ihu)du \quad (4)$$

P(u) can be given by the inverse Fourier transform of temperature factors. On the other hand, anharmonic potential V(u) introduced P(u) by the approximation of the Boltzman distribution function, as expressed below.

$$P(u)=\exp[-V(u)/k_BT]/\int\exp[-V(u)/k_BT]du \quad (5)$$

where k_B indicates the Boltzman constant.

The anharmonic potential V(u) based on one particle potential can be derived from thermal parameters (Willis, 1969, Zuker and Schurz, 1982; Kontio and Stevens, 1982). The anharmonic potential parameters of atomic thermal vibration are calculated from by β_{pq}, γ_{pqr} and δ_{pqrs} coefficients based on the one-particle potential model.

It is noted that the harmonic oscillator model can not give the thermal expansion. Then the anharmonic potential can generate the true atomic thermal displacement, resulting in the thermal expansion of cell volume (Yamanaka et al. 1984; Yamanaka and Morimoto, 1996).

Table 4 shows the interatomic distances calculated from the structure parameters converged by full matrix least-squares refinement including anharmonic thermal parameters. All distances are a little smaller than those data obtained from Rietveld powder profile fitting (Hill and Jackson, 1990).

Discussion

The ABO_3 perovskite structure is characterized as a three-dimensional framework of corner-linked BO_6

Table 2. Atomic coordinate and temperature factor

temperature		20 °C	192 °C	440 °C	703 °C
Sc	x	-0.0206(1)	-0.0204(1)	-0.0198(1)	-0.0206(1)
	y	0.0701(1)	0.0697(8)	0.0689(1)	0.0680(3)
	z	0.250	0.250	0.250	0.250
△ (Å)		0.381	0.379	0.374	0.369
B_{iso}		0.521	0.701	0.887	1.623
$<u_{iso}^2>$ (Å^2)		0.00659	0.00899	0.01123	0.02105
Al	x	0.0	0.0	0.0	0.0
	y	0.5	0.5	0.5	0.5
	z	0.0	0.0	0.0	0.0
△ (Å)		0.0	0.0	0.0	0.0
B_{iso}		0.660	0.819	0.925	1.587
$<u_{iso}^2>$ (Å^2)		0.00835	0.01037	0.01172	0.02010
O1	x	0.1201(4)	0.1195(4)	0.1194(5)	0.1181(10)
	y	0.4550(4)	0.4550(3)	0.4552(5)	0.4545(9)
	z	0.25	0.25	0.25	0.25
△ (Å)		0.6381	0.6354	0.6363	0.6337
B_{iso}		0.619	0.784	0.902	1.598
$<u_{iso}^2>$ (Å^2)		0.00784	0.00993	0.01142	0.02024
O2	x	0.6909(3)	0.6903(2)	0.6901(4)	0.6900(7)
	y	0.3059(3)	0.3063(2)	0.3063(3)	0.3057(6)
	z	0.0611(2)	0.0610(5)	0.0608(3)	0.0608(5)
△ (Å)		1.0802	1.0785	1.0800	1.0817
B_{iso}		0.649	0.815	0.968	1.589
$<u_{iso}^2>$ (Å^2)		0.00822	0.01032	0.01226	0.02012
maximum 2θ angle		90	75	75	75
No. of reflect.(obs)		483	380	385	375
No. of reflect (used)		464	352	347	288
R-facor		0.0201	0.0196	0.0223	0.0383
Rw-factor		0.0253	0.0240	0.0352	0.0499

$\Delta(\text{Å}) = \sqrt{a^2(x_i-x_o)^2+b^2(y_i-y_o)^2+c^2(z_i-z_o)^2}$

Table 3. Anisotropic temperature factors up to fourth

temperature	20° C	192° C	440° C	703° C
Sc				
β_{11} x10^5	500(9)	885(29)	1028(75)	1695(112)
β_{22} x10^5	499(10)	610(35)	571(86)	1289(125)
β_{33} x10^5	255(16)	356(40)	490(107)	853(154)
β_{12} x10^5	-23(9)	-25(18)	-47(41)	-99(78)
β_{13} x10^5	0	0	0	0
β_{23} x10^5	0	0	0	0
γ_{111} x10^6	12(10)	58(28)	59(40)	137(80)
γ_{222} x10^6	25(14)	38(34)	69(44)	101(92)
γ_{112} x10^6	-5(11)	-14(32)	-21(47)	-15(98)
γ_{122} x10^6	4(8)	8(30)	12(40)	16(81)
γ_{133} x10^6	-8(9)	-2(30)	-19(49)	-21(87)
γ_{233} x10^6	21(10)	31(28)	42(47)	60(92)
δ_{1111} x10^7	20(17)	32(34)	42(52)	70(100)
δ_{2222} x10^7	12(20)	18(31)	12(55)	50(110)
δ_{3333} x10^7	15(21)	22(42)	37(65)	60(182)
Al				
β_{11} x10^5	647(12)	1006(23)	1113(69)	1741(120)
β_{22} x10^5	723(18)	610(30)	736(80)	1471(134)
β_{33} x10^5	270(29)	389(42)	419(82)	679(172)
β_{12} x10^5	-8(14)	-9(23)	-7(61)	-25(80)
β_{13} x10^5	9(12)	12(28)	10(65)	32(90)
β_{23} x10^5	15(21)	17(24)	64(78)	66(94)
δ_{1111} x10^7	26(20)	41(45)	77(70)	196(111)
δ_{2222} x10^7	22(22)	29(42)	40(79)	152(132)
δ_{3333} x10^7	17(29)	34(30)	90(71)	87(121)

octahedra. In the ideal cubic perovskite (Pm3m, z=1), 12-fold coordinated A-cation has a complex form of hexahedron {100} and octahedron {111}. All 14 polyhedral faces are shared with eight B-site and six A-site polygons. A-cation has 8 equivalent and 4 other equivalent bond lengths. BO_6 octahedra share their faces with AO_{12} polygon and the B-O bond lengths directly define the lattice constant, because they are situated parallel to the cell edges.

In the case of $ScAlO_3$ orthorhombic (Pbnm, z=4) perovskite which is visualized by enormous deformation from cubic symmetry, the Sc atom is surrounded by 12 oxygen neighbors ranging from 2.06Å to 3.4Å. It can be defined as 8-fold coordination due to the tilting of adjacent octahedra (Figure 2). Four A-O distances among twelve are elongated over 3.0Å, resulting in little bonding characters (Brown, 1985). This polyhedron shares only edges with BO_6 octahedra instead of sharing faces. Hence the cell volume partly consists of the void space in addition to AO_8 and BO_6 polyhedral spaces. The void space formed by an oxygen cage occupies more than 40% of the unit cell volume, as shown in Table 4. The thermal expansion or compression of the cell volume is a summation of the change of those individual spaces.

Many aluminate and silicate perovskites have an orthorhombic symmetry. The relative interatomic distances for A-O and B-O bonds and tilting and rotation of octahedron characterize them. The present high temperature experiment and high-pressure study from Ross (1998) show the effect of thermal expansion and compression in the bond lengths and site-volumes. In both cases each cation site volume of $ScAlO_3$ seems to be almost homogeneously expanded by heating and compressed by pressurization.

rank tensors of Gram-Charlier expansion

temperature	20° C	192° C	440° C	703° C
O1				
β_{11} x10^5	579(15)	1042(35)	1129(73)	1981(140)
β_{22} x10^5	680(17)	606(40)	738(80)	1430(154)
β_{33} x10^5	265(23)	323(42)	377(87)	603(172)
β_{12} x10^5	-53(20)	-48(30)	-88(67)	-27(87)
β_{13} x10^5	0	0	0	0
β_{23} x10^5	0	0	0	0
γ_{111} x10^6	32(15)	68(34)	80(56)	172(97)
γ_{222} x10^6	25(18)	41(40)	69(62)	121(81)
γ_{112} x10^6	-15(30)	-18(42)	-23(70)	-32(78)
γ_{122} x10^6	12(32)	8(37)	12(75)	16(80)
γ_{133} x10^6	-8(27)	-10(40)	-9(82)	-11(98)
γ_{233} x10^6	1(32)	3(43)	4(71)	10(92)
δ_{1111} x10^7	17(14)	22(34)	32(49)	52(90)
δ_{2222} x10^7	21(20)	28(42)	42(52)	70(89)
δ_{3333} x10^7	6(25)	12(47)	37(60)	30(110)
O2				
β_{11} x10^5	621(20)	989(32)	1130(80)	1553(143)
β_{22} x10^5	636(23)	569(42)	683(99)	1200(192)
β_{33} x10^5	312(33)	412(60)	500(92)	916(187)
β_{12} x10^5	-83(22)	-97(55)	-97(62)	-56(143)
β_{13} x10^5	27(20)	41(42)	41(70)	99(123)
β_{23} x10^5	-66(25)	-63(40)	-115(77)	-147(140)
γ_{111} x10^6	78(31)	99(47)	134(59)	203(97)
γ_{222} x10^6	69(36)	82(45)	111(68)	192(89)
γ_{333} x10^6	42(30)	54(40)	92(70)	142(110)
γ_{112} x10^6	-21(28)	-34(42)	-41(52)	-74(98)
γ_{122} x10^6	20(29)	12(37)	36(54)	65(90)
γ_{113} x10^6	11(27)	27(40)	42(67)	52(89)
γ_{133} x10^6	-20(30)	-12(45)	-39(52)	-74(80)
γ_{223} x10^6	19(33)	12(37)	31(57)	25(78)
γ_{233} x10^6	2(24)	13(50)	27(60)	53(88)
δ_{1111} x10^7	32(19)	30(30)	24(59)	42(108)
δ_{2222} x10^7	10(16)	9(31)	31(70)	42(90)
δ_{3333} x10^7	28(20)	45(38)	72(68)	121(110)

Thermal expansion coefficient

It is natural that all structure changes with temperature are caused by thermal effect on the nature of bonding in ionic crystals and thermal vibrations of atoms. Density of electronic state and overlapping electron cloud between ions should be changed. These changes induce the deformation of polyhedra and polyhedral configuration. Finally symmetry change brings thermal phase transformation.

The structure of $ScAlO_3$ is greatly distorted from the cubic perovskite symmetry and most of variable atomic coordinates shifted from the crystallographic special positions. This distortion brings the deforma-

tion of polyhedra of ScO_8 and AlO_6 and tilting and rotation of the octahedral linkage, which can be seen from the polyhedral linkages of the structure (Figure 2). As easily seen from Table 2, all temperature factors of β_{pq} of Sc, Al, O1 and O2 atoms show almost same order tensors. Anions, O1 and O2, show a large anisotropy of their thermal ellipsoids in comparison with those of cations, as seen from Figure 2. At higher temperatures, the larger anisotropy of thermal vibration of O1 and O2 atoms probably induces an enhancement of tilting and rotation angle of AlO_6.

The bond angle $\angle$Al-O1-Al is an indicator (ϕ) of the tilting of the octahedra against the c axis and that $\angle$Al-O2-Al angle is that of the rotation (ψ) of octahedra around the c axis. Even cations exhibit surprisingly large isotropic temperature factors, B_{iso}. This is quite a different feature from ordinary ionic crystals. However, higher order anisotropic anharmonic temperature factors of γ_{pqr} and δ_{pqrrs} of O1 and O2 atoms are noticeably increased with temperature, which give a large influence on anharmonic parameters. Thermal changes of perovskite framework are controlled by anharmonic thermal motion of atoms, which changes ϕ and ψ angles of AlO_6 octahedra and also the thermal changes of atomic positions and lattice constants are given by statistical positional density owing to the anharmonic atomic thermal-motion. The orthorhombic unit cell dimensions of $ScAlO_3$ as a function of temperature (T) are well fitted to the following quadratic equation ($1+\alpha T+\beta T^2$) by a least-squares calculation because of anharmonic thermal vibration of atoms;

$$a(\text{Å}) = 4.935(1+6.723\times10^{-6}T+4.391\times10^{-9}T^2)$$
$$b(\text{Å}) = 5.230(1+4.293\times10^{-6}T+2.516\times10^{-9}T^2)$$
$$c(\text{Å}) = 7.199(1+3.846\times10^{-6}T+2.461\times10^{-9}T^2)$$

These thermal expansion coefficients clearly indicate the anisotropy of the cell edges. The cell edge ratios of $\sqrt{2}a/c$, $\sqrt{2}b/c$ and a/b (Table 1) explain that the orthorhombic framework does not change its symmetry in the temperature range of the present study. However, $\sqrt{2}a/c$, and $\sqrt{2}b/c$ imply a tendency toward higher symmetry of $a=b$. The tendency can be visualized in Figure 3.

It is noted that an ideal harmonic thermal oscillation of atoms causes neither thermal expansion nor any structure change. At relatively low temperatures, anharmonicity is not significant factor, especially for materials having high Debye temperature (θ_D). Then the thermal expansion coefficients of $ScAlO_3$ are much smaller than those of halide perovskites, such as $NaMgF_3$ (Zhao et al., 1993a).

The single crystal structure refinement revealed that those atomic coordinates do not change within the experimental temperature range. However, from data of Δ(Å) in Table 2 the orthorhombic structure becomes only a little closer to a higher symmetry. At higher temperature the polyhedral deformation of ScO_8 is slightly relaxed by thermal motion of atoms. On the other hand, AlO_6 octahedron remains a fairly good regular octahedron. The expansions of mean bond distances are represented by the following equations, respectively:

$$d(ScO)_8 = 2.2693(1+0.4496\times10^{-5}T+2.6892\times10^{-9}T^2)$$
$$d(ScO)_{12} = 2.6034(1+0.4323\times10^{-5}T+1.0887\times10^{-9}T^2)$$
$$d(AlO)_6 = 1.8984(1+0.4333\times10^{-5}T+1.3773\times10^{-9}T^2)$$

Shorter bonds indicate generally less thermal expansion in each cation site than those having longer ones. The bond lengths of cations having a higher coordination number become longer with temperature than those having a lower coordination. That is why the expansion coefficient α of $d(AlO)_6$ is smaller than that of $d(ScO)_8$.

The unit cell volume change of $ScAlO_3$ with temperatures does not show a linear expansion but well accords with the quadratic equation:

$$V(T)/V_{293} = 1+1.510\times10^{-5}T+9.2181\times10^{-9}T^2.$$

The expansion of $ScAlO_3$ is much smaller than that of $MgSiO_3$ perovskite measured up to 840 K by Knittle et al. (1986). The latter perovskite has an enormous expansion, which proves the instability at high temperature under atmospheric pressure.

The volume of ScO_8 is given from the summation of 12 tetrahedra around the Sc ion. Void space is introduced by the subtraction of total volumes of ScO_{12} and AlO_6 from the unit cell volume. The thermal expansion coefficients of all these volumes are

$$ScO_8 \quad V(T)/V_{293} = 1+1.545\times10^{-5}T+10.996\times10^{-9}T^2$$
$$ScO_{12} \quad V(T)/V_{293} = 1+1.805\times10^{-5}T+7.163\times10^{-9}T^2$$
$$AlO^6 \quad V(T)/V_{293} = 1+1.466\times10^{-5}T+7.440\times10^{-9}T^2$$
$$\text{Void} \quad V(T)/V_{293} = 1+1.494\times10^{-5}T+8.165\times10^{-9}T^2.$$

All polyhedral volumes show almost the same thermal expansion including the void space. The volume changes of ScO_{12} and AlO_6 polyhedra together with that of the void space are shown in Figure 4. As seen from the figure, the void space and ScO_8 have a very similar volume and the thermal expansion. The expansions of ScO_8 and the void space are significant for the cell volume expansion. Because of their large volume fractions in the unit cell, the influence of the void space on the volume expansion is remarkable. Recalculation from structure analyses under compression (Ross, 1998) shows all three volumes, ScO_8, AlO_6 and void space

Table 4. Interatomic distance and site volume

temperature	20° C	192° C	440° C	703° C
Sc-O1	2.066(2)	2.071(2)	2.071(3)	2.080(5)
Sc-O1	2.131(2)	2.132(2)	2.140(3)	2.141(5)
Sc-O1	3.291(2)	3.291(3)	3.291(3)	3.294(5)
Sc-O1	3.019(2)	3.030(4)	3.030(4)	3.036(6)
Sc-O2 (x2)	2.324(1)	2.330(1)	2.341(2)	2.349(4)
Sc-O2 (x2)	2.113(1)	2.112(1)	2.115(2)	2.119(4)
Sc-O2 (x2)	2.555(1)	2.555(2)	2.558(2)	2.562(4)
Sc-O2 (x2)	3.396(2)	3.399(1)	3.401(2)	3.402(4)
MEAN (8)	2.273(2)	2.275(2)	2.280(2)	2.285(4)
MEAN (12)	2.607(2)	2.609(2)	2.614(2)	2.617(4)
Al-O1 (x2)	1.909(1)	1.910(1)	1.914(1)	1.915(2)
Al-O1 (x2)	1.885(1)	1.888(1)	1.892(2)	1.899(3)
Al-O1 (x2)	1.885(2)	1.888(2)	1.892(3)	1.899(4)
MEAN(6)	1.901(1)	1.903(1)	1.906(2)	1.909(3)
∠Al-O1-Al	141.10	141.12	141.15	141.35
∠Al-O2-Al	142.91	142.8	142.84	142.92
V(cell)	185.905(6)	186.379(1)	187.432(1)	188.634(2)
$V(Sc)_8$ (x2)	19.633(3)	19.681(3)	19.805(3)	19.941(5)
$V(Sc)_{12}$ (x2)	37.334(3)	37.392(3)	37.685(4)	37.894(5)
$V(Al)_8$ (x4)	9.144(2)	9.163(2)	9.215(3)	9.266(6)
Void space	70.797	71.003	71.56	71.806
$V(Sc)_{12}/V(Al)_8$	4.083	4.081	4.086	4.089
$V(Sc)_8/V(Al)_8$	2.148	2.146	2.146	2.151
Void/V(cell)	0.3808	0.3811	0.3818	0.3807
tolerance(12)	0.9698	0.9696	0.9695	0.9693
tolerance(8)	0.8454	0.8453	0.8457	0.8463

The tolerance factor is expressed by t (=Sc-O/$\sqrt{2}$Al-O).

decrease monotonously with pressure increase. Accordingly, no structure change of $ScAlO_3$ can be expected by pressurization.

Polymorphic symmetries of unquenchable high-pressure ABO_3 perovskites are mostly defined by charges and ionic sizes of A^{2+} and B^{4+} cations in terms of the tolerance factor (Leinenweber et al., 1991, 1994). Studies of germanate perovskites under high-pressure indicates the various transformations by those cation radius ratio and heating process (Hattori et al., 1999).

Rare-earth aluminate perovskites ($RAlO_3$) may undergo polymorphic transitions by heating or pressurization because they contain the large cations of A^{3+} with ionic radii exceeding 0.95Å. However, Sc^{3+} having 0.87Å is too small to make the transition.

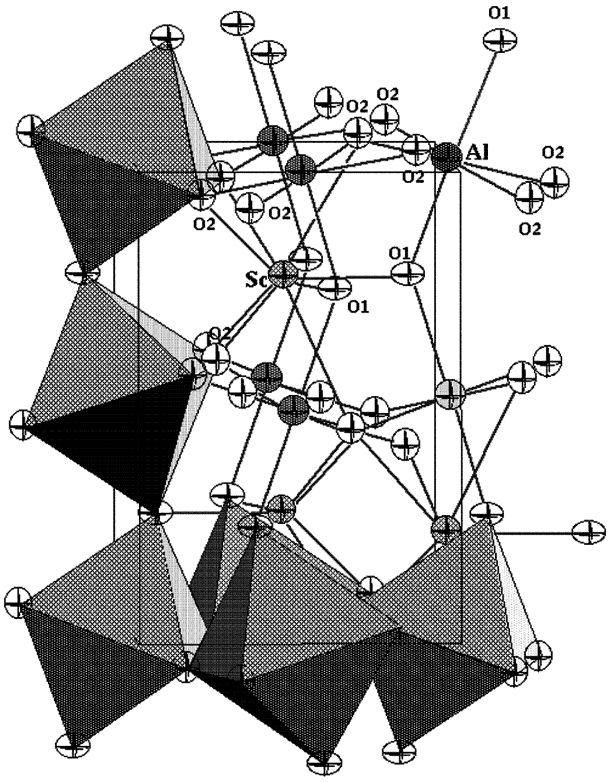

Figure 2 Crystal structure of $ScAlO_3$ at ambient condition. Polyhedral linkage is partly expressed in order to visualize the tilting and rotation of octahedra. Thermal ellipsoids indicate the thermal motion of atoms. Anisotropic thermal motions of O1 and O2 give a large effect on the tilting and rotation of octahedra.

Distortion of polyhedra

The change of the perovskite structure with increasing temperature is naturally related to the relative volume expansions of two cation polyhedra. The larger ϕ and ψ angles of octahedra at higher temperature relax the deformations of the Al and Sc polyhedra. The tolerance factor t (=Sc–O/$\sqrt{2}$Al–O) is presented in Table 4. The value increases only a little with temperature. Thermal expansion of Sc–O of the large Sc cation is greater than Al–O of the small Al cation in $ScAlO_3$ perovskite. This makes the tolerance factor a little smaller. Polyhedral thermal expansion at much higher temperatures than that of the present experimental condition may enhance the symmetry from the distorted orthorhombic perovskite to tetragonal and further to cubic.

The tilting angle ϕ of the octahedra against the c axis and the rotation ψ around the axis are slightly raised with increasing temperature. If the tendency extends further with 4-fold rotation along the c axis, the orthorhombic structure of Pbnm is changed to the tetragonal perovskite having a space group of I4/mcm. If the angles of ∠Al–O1–Al and ∠Al–O2–Al become 180° and the octahedron has an ideal symmetry, perovskite will be transformed to the cubic structure having the space symmetry of Pm3m.

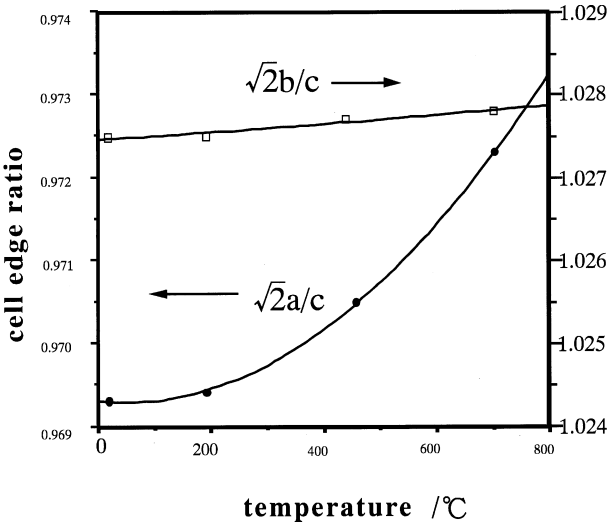

Figure 3 Thermal change of the cell edge ratio.

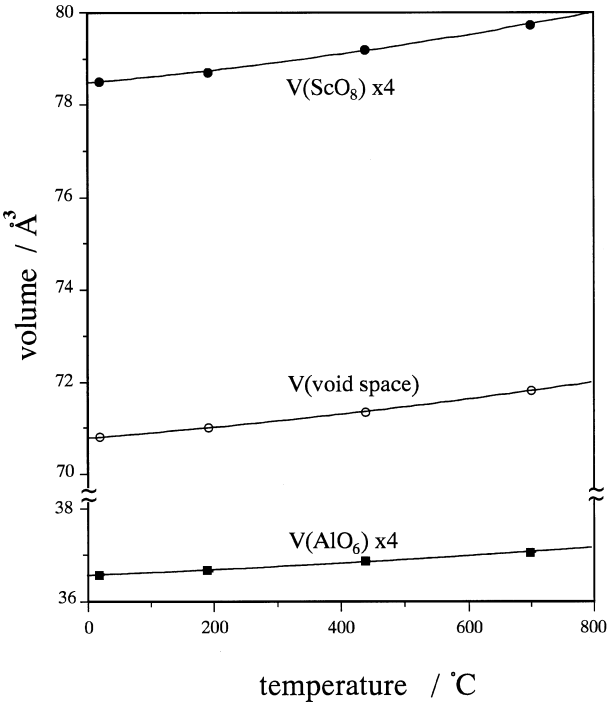

Figure 4 Volume expansions of void space, ScO_8 and AlO_6 polyhedra.
The volume of ScO_8 is calculated from the summation of 12 tetrahedra around Sc ion. Void space is introduced by the subtraction of total volumes of ScO_8 and AlO_6 from the unit cell volume.

The present single-crystal structure refinements of $ScAlO_3$ at various temperatures elucidated that ellipsoids represent the atomic displacements due to the thermal vibration and proved the motivation of the structure change. Temperature factors of O1 and O2 show the strong anisotropy and enhance the tilting and rotation of the octahedra-linkage with increasing temperature. The isotropic temperature factor B_{iso} and $\langle u^2 \rangle$ are calculated from the anisotropic temperature factors β_{pq}. B_{iso} of O2 larger than that of O1 probably indicates a larger degree of rotation of AlO_6 octahedra in comparison with tilting motion.

The thermal expansion of the cell volume is introduced from those of the cation polyhedra, which should be related the bond strength. The bonding energy defines the elastic stiffness due to the thermal stress. Bass (1984) measured the adiabatic single-crystal elastic moduli of $ScAlO_3$ by means of Brillouin spectroscopy. These constants show the stiffness parameters, which relate not only to the softness of interatomic bond strength but also the rotation and tilting of octahedra.

References

Bass, J. (1984) Elastic of single-crystal $SmAlO_3$, $GdAlO_3$ and $ScAlO_3$ perovskites. Physics of the Earth and Planetary Interiors. 36, 145-156.

Brown G.E., Sueno, S. and Prewitt, C.T. (1973) A new single-crystal heater for the precession camera and four-circle diffractometer. American Mineralogist, 58, 698-704.

Brown, I.D. and Altermatt, D. (1984) Bond valence parameters obtained from a systematic analysis of the inorganic crystal structure database. Acta Crystallography, B41, 244-247.

Galasso, F.S. (1970) Structure and properties of inorganic solids. International Series of Monographs in Solid State Physics Vol. 7. Pergamon Press Inc.

Glazer, A.M. (1972) The classification of titled octahedra in perovskites. Acta Crystallography, B28, 3384-3392.

Glazer, A.M. (1975) Simple ways of determining perovskite structure. Acta Crystallography, A31, 756-763.

Hattori, T., Matsuda, T., Tsuchiya, T., Nagai, T. and Yamanaka, T. (1999) Clinopyroxene-perovskite phase transition of $FeGeO_3$ under high pressure and room temperature. Physics and Chemistry of Minerals, 26, 212-216.

Hazen, R.M. and Finger, L.W. (1982) Comparative crystal chemistry. J. Wiley & Sons, New York.

Hill, R.J. and Jackson, I. (1990) The thermal expansion of $ScAlO_3$-A silicate perovskite analogue. Physics and Chemistry of Minerals, 17, 89-96.

Ito, E. and Matsui, Y. (1978) Synthesis and crystal-chemical characterization of $MgSiO_3$ perovskite. Earth and Planet Science Letters, 38, 443-450.

International Tables for X-ray Crystallography, Vol. IV (1974). 324-331.

Johnson, C.K. and Levy, H.A. (1974) International Table for X-ray crystallography, Vol. IV, 311-36. Birmingam; Kynoch Press.

Knittke, E., Jeanloz, R. and Smith, G.L. (1986) Thermal expansion of silicate perovskite and stratification of the Earth's mantle. Nature, 319, 214-216.

Kontio A. and Stevens, E.D. (1982) Determination of the one-particle potential for an atom with highly anharmonic thermal motion. Acta Crystallography, A38, 623-629.

Kudoh, Y., Ito, E. and Takeda, H. (1987) Effect of pressure on the crystal structure of perovskite-type $MgSiO_3$. Physics and Chemistry of Minerals, 14, 350-354.

Leinenweber, K., Wang, Y., Yagi, T. and Yusa, H. (1994) An unquenchable perovskite phase of $MgGeO_3$ and comparison with $MgSiO_3$ perovskite. American Mineralogist, 7, 197-199.

Leinenweber, K., Utsumi, W., Tsuchida Y., Yagi, T. and Kurita K. (1991) Unquenchable high-pressure perovskite polymorphs of $MnSnO_3$ and $FeTiO_3$. Physics and Chemistry of Minerals, 18, 244-250.

Liu, L.G. (1978) Orthorhombic perovskite phases observed in olivine, pyroxene and garnet at high pressures and temperatures. Physics of the Earth Planetary Interiors, 11, 289-298.

Merezio, M., Dernier, P.D. and Remeika, J.P. (1972) The crystal structure of orthorhombic $SmAlO_3$ and trigonal $NbAlO_3$. Journal Solid State Chemistry, 4, 11-19.

Reid, A.F. and Ringwood, A.E. (1975) High pressure modification of $ScAlO_3$ and some geophysical implication. Journal of Geophysical Research, 80, 3363-3370.

Ringwood, A.E. (1962) Mineralogical constitute of the deep mantle. Journal of Geophysical Research, 67, 4005-4010.

Ross, N. (1998) High pressure study of $ScAlO_3$ perovskite. Physics and Chemistry of Minerals, 25, 597-602.

Ross, N. and Hazen, R.M. (1990) Single Crystal X-ray diffraction study of $MgSiO_3$ perovskite from 77 to 400 K Physics and Chemistry of Minerals, 16, 415-420.

Sasaki, S. (1987) A Fortran program for the least-squares refinement of crystal structures, National Laboratory foe High Energy Physics, Japan.

Sasaki, S., Prewitt, C.T. and Libermann, R.C. (1983) The crystal structure of $CaGeO_3$ perovskite and the crystal chemistry of the $GdFeO_3$ type perovskites. American Mineralogist, 68, 1189-1198.

Sinclair, W., Eggleton, R.A. and Ringwood, A.E. (1979) Crystal synthesis and structure refinement of high-pressure $ScAlO_3$ perovskite. Zeitschrift für Kristallographie, 149, 307-314.

Susaki, J., Konno, M. and Akimoto, S. (1985) High-pressure synthesis and structural refinement of $CdFeO_3$ ilumenite. Zeitschrift für Kristallographie, 171, 243-252.

Willis, B.T.M. (1969) Lattice vibration and the accurate determination of structure factors for the elastic scattering of X-rays and neutron. Acta Crystallography, A25, 277-300.

Yagi, T., Mao, H. and Bell, P.M. (1978) Structure and crystal chemistry of perovskite-type $MgSiO_3$. Physics and Chemistry of Minerals, 3, 97-110.

Yamanaka, T.,Takeuchi, Y. and Sadanaga, R. (1981) Gas-flame, high-temperature apparatus for single crystal X-ray diffraction studies. Zeitschrift für Kristallographie, 154, 147-153.

Yamanaka, T., Takeuchi, Y. and Tokonamai, M. (1984) Anharmonic thermal vibration of atoms in $MgAl_2O_4$

spinel at temperature up to 1933K. Acta Crystallography, B40, 96–102.

Yamanaka, T. and Morimoto, S. (1996) Isotope effect on anharmonic thermal atomic vibration and κ-refinement of ^{12}C and ^{13}C diamond. Acta Crystallography, B52, 232–238.

Yamanaka, T. and Takeuchi, Y. (1983) Order-disorder transition in $MgAl_2O_4$ spinel at high temperatures up to 1700°C. Zeitschrift für Kristallographie, 165, 65–78.

Zhao, Y., Weidner, D.J., Parise, J.B. and Cox, D.E. (1993a) Thermal expansion and structural distortion of perovskite data for $NaMgF_3$ perovskite. Part I. Physics of the Earth and Planetary Interiors, 1–16.

Zhao, Y., Weidner, D.J., Parise, J.B. and Cox, D.E. (1993b) Critical phenomena and phase transition of perovskite data for $NaMgF_3$ perovskite. Part II. Physics of the Earth Planetary Interiors, 17–34.

Zuker, U. and Shurz, H. (1982) Statistical approaches for the treatment of anharmonic motion in crystals. 1. A comparison of the most frequently used formalism of anharmonic thermal vibrations. Acta Crystallography, A38, 563–568.

Manuscript received; 12 July, 2000
Manuscript accepted; 31 October, 2001